Solid State Ionics 180 (2009) 822–826

Contents lists available at ScienceDirect

Solid State Ionics

journal homepage: www.elsevier.com/locate/ssi

Impedance spectroscopy study of the sintering of yttria-stabilized zirconia/magnesia composites

F.C. Fonseca [a,*], D.Z. de Florio [b], R. Muccillo [a]

[a] Instituto de Pesquisas Energéticas e Nucleares, 05508-000, São Paulo, SP, Brazil
[b] Universidade Federal do ABC, 09210-170, Santo André, SP, Brazil

ARTICLE INFO

Article history:
Received 19 September 2008
Received in revised form 23 January 2009
Accepted 1 February 2009

Keywords:
Sintering
Impedance spectroscopy
Zirconia
Composite
Fuel cell

ABSTRACT

In the present study, the sintering of $(ZrO_2{:}8\ mol\%Y_2O_3)_{1-m}$–$(MgO)_m$, YSZ–*m*Mg composites, with *m* in the 0–30 mol% range, has been investigated by impedance spectroscopy (IS), dilatometry, and X-ray diffraction. Impedance diagrams were collected at 400 °C after heating the green compacts up to a selected sintering temperature, which was increased stepwise from 800 to 1400 °C. The combined experimental results revealed that the samples can be separated in two categories: below and above the solubility limit of MgO in the YSZ ($m \sim 10$). Moreover, important microstructural features associated with both the sintering process and solid solution formation of YSZ–*m*MgO samples were correlated to the electrical properties inferred by IS.

© 2009 Elsevier B.V. All rights reserved.

1. Introduction

Solid electrolytes based on the stabilized zirconia have been extensively studied due to both intriguing properties and technological interest in devices such as oxygen sensors and solid oxide fuel cells, which rely on the high ionic conductivity of this ceramic material [1–3]. The electrical conductivity of stabilized zirconia has been related to both the ionic radius and the concentration of the dopant cation, usually in the 5–20 mol% range, and to the defect association between dopants and lattice cations [1]. Usually, maximum electrical conductivity is observed for dopants having ionic radius comparable to that of zirconium and for molar concentration close to the minimum necessary to stabilize the cubic structure of the zirconia [4]. Further increasing the concentration of the dopant generates more oxygen vacancies which do not contribute to the ionic transport [4]. A high concentration of lattice defects, above a certain maximum value that depends on the stabilizer cation, leads to defect interactions that decrease the oxygen ion transport. Amongst the typical oxides used as stabilizers of the cubic and tetragonal structures of zirconia, Y_2O_3 (~3–10 mol%) and MgO (~5–15 mol%) are known for high electrical conductivity and thermal shock resistance, respectively [1,4,5]. In this context, the possibility of tailoring the properties of zirconia-based electrolytes by co-doping is an important aspect regarding such electrolytes [6].

The ZrO_2–Y_2O_3–MgO ternary system has already been studied specially regarding the phase diagram, the diffusion-induced grain boundary migration, improved thermal stability for oxygen sensors, and structural applications of partially stabilized systems [7–11]. More recently, MgO doping in YSZ was pointed as a possible way to better match the thermal expansion coefficient (TEC) of the electrolyte with adjacent components of the solid oxide fuel cell (SOFC) [12]. However, investigations on the electrical properties of this ternary system are seldom found [13].

Impedance spectroscopy has been used as a standard tool for the study of the electrical properties of zirconia-based solid electrolytes. The separation, on the frequency domain, of the electrical response arising from different microstructural constituents such as grain, grain boundary, pore, and second phases allows for the analysis of distinct processes occurring in such materials. In this context, the sintering behavior of YSZ electrolytes has been studied by impedance spectroscopy [14,15]. Impedance data revealed important information concerning pore elimination and grain growth during sintering of yttria-stabilized zirconia [14–16].

In the present work, the sintering of YSZ–MgO compacts was studied by impedance spectroscopy. The electrical measurements revealed important features concerning the YSZ–MgO system such as the onset of linear shrinkage and the formation of solid solution between the two ceramic phases. Such features were found to be in excellent agreement with both dilatometry and high temperature X-ray diffraction analyses.

2. Experimental

Composite samples of $(ZrO_2{:}8\ mol\%Y_2O_3)_{1-m}$–$(MgO)_m$, YSZ–*m*Mg, with *m* ranging from 0 to 30 mol%, were prepared by a liquid mixture technique. This process consists in the evaporation of a dispersion of YSZ (Tosoh, Japan) powder in a solution of magnesium

* Corresponding author. Tel.: +55 11 3133 9282; fax: +55 11 31339193.
E-mail address: fcfonseca@ipen.br (F.C. Fonseca).

0167-2738/$ – see front matter © 2009 Elsevier B.V. All rights reserved.
doi:10.1016/j.ssi.2009.02.010

nitrate (Vetec, Brazil) and isopropanol. The liquid mixture was heated on a hot plate at ~60 °C under vigorous stirring to evaporate the ethanol. This mixture was calcined at 500 °C for 1 h for the formation of MgO, as inferred from thermogravimetric analysis (TG, not shown). According to TG analysis, after ethanol evaporation MgO is formed at ~425 °C and no further mass losses were observed up to 600 °C. In addition, TG data indicate that the nominal fraction of MgO is close to the experimental one within 10% of experimental accuracy. X-ray diffraction analyses confirmed that the samples consist of a mixture of YSZ and MgO after heat treatment at 500 °C.

The resulting powder was ground in an agate mortar for ~15 min. The specimens were analyzed by X-ray diffraction (Bruker-AXS D8 Advance diffractometer) at room temperature, using CuK_α radiation. The powders were also analyzed by high temperature X-ray diffraction up to 1250 °C. An Anton Paar (model HTK-16) high temperature sample chamber with a platinum heating attachment and a Braun PSD X-ray detector were used. A Pt–10%RhPt thermocouple monitors and control the temperature within ~1 °C of the set temperature. The platinum strip sample holder was coated with 100 to 150 mg of the samples. Cylindrical pellets were prepared by uniaxial and isostatic pressing at 100 MPa and 200 MPa, respectively. Green densities of the compacts with $m \leq 10$ were found to be close to ~50% of the theoretical value calculated by the rule of mixtures, and slightly lower values were measured for specimens with higher MgO content.

The sintering of the YSZ–*m*Mg samples was studied by the impedance spectroscopy (IS) technique. Platinum contacts were painted on the parallel surfaces of green compacts with Degussa Pt paste and dried at 100 °C overnight. The sample was placed in an alumina sample holder between two platinum disks and close to the measuring tip of a type S thermocouple. The electrical contact was assured by spring-loading the specimen on the alumina rods that support both Pt disks. This sample holder was positioned inside a resistive furnace, and the following sequence was used for different sintering temperatures: *i*) heating up to 800 °C for both curing of Pt contacts and the first sintering temperature; *ii*) cooling down to 400 °C; *iii*) collecting the impedance spectroscopy data corresponding to the sintering temperature; *iv*) heating the specimen to the next sintering temperature, and steps *ii* and *iii* were repeated. Sintering temperatures were stepwise increased from 800 to 1400 °C with heating rate of 10 °C/min, holding time of 0.1 h at the sintering temperature, and 10 °C/min cooling rate to the measuring temperature (400 °C). The IS analyses were carried out in the 5 Hz to 13 MHz, with 100 mV of signal amplitude using an HP 4192A LF impedance analyzer connected to an HP 362 controller. Four impedance diagrams were collected consecutively at 400 °C for each sintering temperature. The impedance diagrams were analyzed by considering a model of two parallel RC circuits connected in series, using a special software [17]. The deconvolution of diagrams into two semicircles was possible above sintering temperatures of ~1000 °C, when the overlap

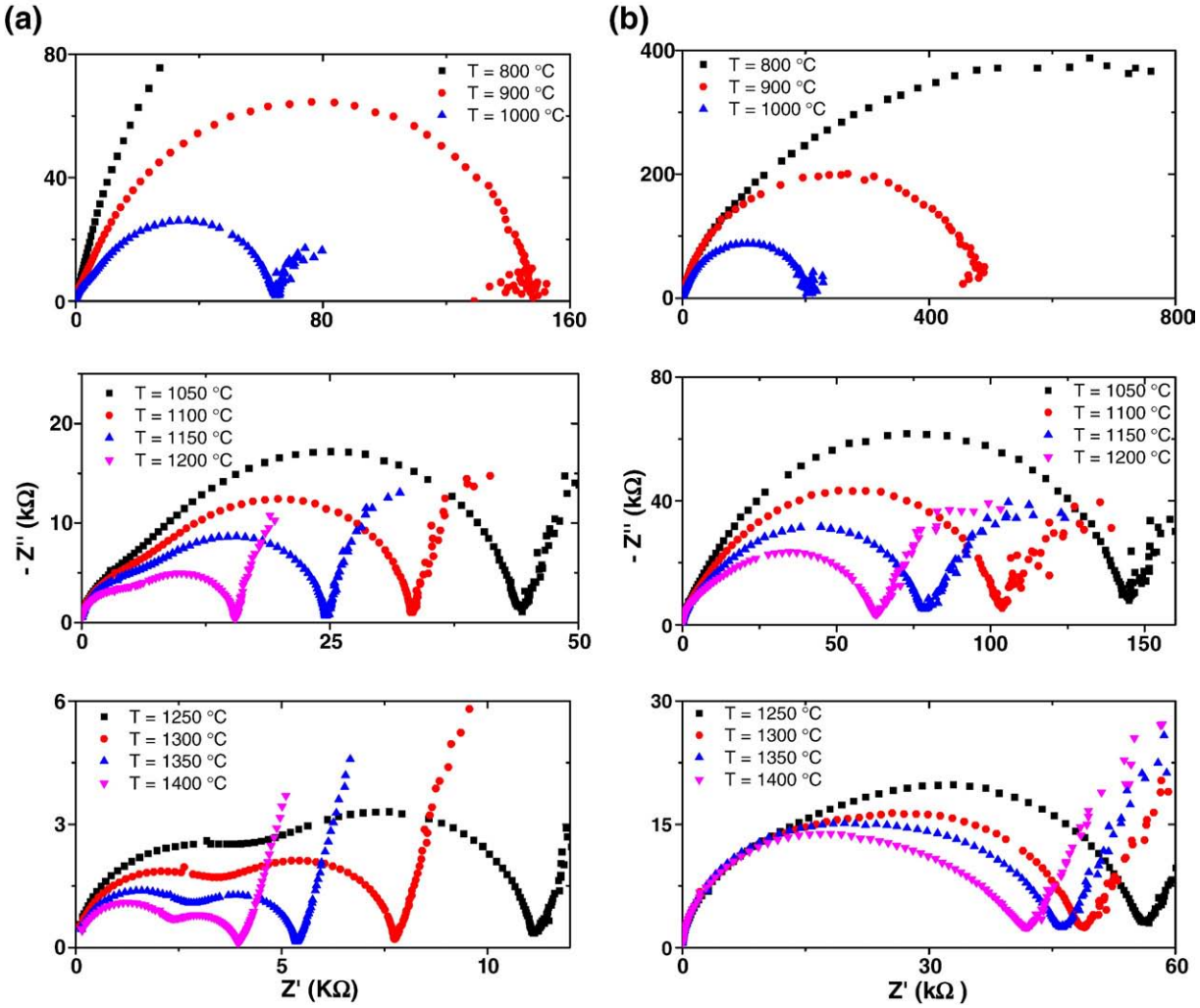

Fig. 1. Impedance diagrams taken at 400 °C, after sintering the green compacts in the 800–1400 °C range, of the samples (a) ZrO_2:8 mol% Y_2O_3–2 mol% MgO and (b) ZrO_2:8 mol% Y_2O_3–30 mol% MgO.

between high and low frequency components is less pronounced. The software provides for both semicircles (high and low frequency ones (*hf* and *lf*, respectively) values of resistance *R*, relaxation frequency ($f_0 = \omega_0/2\pi$), capacitance ($C = 1/R\omega_0$), and the decentralization angle (β), representing the depression of the semicircles from the real axis. The quality of the diagram deconvolution was assured by following the behavior of the fitting quality parameter, calculated by the software, and by monitoring both the magnitude and temperature dependence of the resulting fitted parameters. The presented results correspond to the average values of the four sets of fitted parameters, and error bars represent the standard deviation. The resistance values were normalized to the final dimensions of the specimens after sintering.

Dilatometry analyses of green compacts were performed up to 1500 °C with a heating rate of 8 °C/min in air using a Netzsch DIL 402 E/7 apparatus.

3. Results and discussion

The impedance spectroscopy diagrams taken during sintering the YSZ–*m*MgO samples are displayed in Fig. 1(a) and (b) for the samples with $m = 2$ and 30, respectively. A first important difference between the two compositions is the total electrical resistance (*Rtot*), which is one order of magnitude higher for the $m = 30$ sample, as it would be expected for a composite with a higher volume fraction of the insulating phase. For the low MgO content sample ($m = 2$), the temperature dependence of impedance diagrams is equivalent to the one of pure YSZ. At low sintering temperature ($T < 1000$ °C), only one semicircle, with relaxation frequency within the range of the low frequency component ($f_0 lf \sim 10^5$ Hz), is observed. With increasing sintering temperature a deviation in the high frequency range of the impedance diagram indicates that the separation into two semicircles starts to occur at the sintering temperature ~1000 °C (Fig. 1a). The oxygen ion conductivity, measured by IS, is a highly sensitive probe that reveals the beginning of neck formation at early sintering stages [18]. Further increasing the sintering temperature results in rapid decrease of the electrical resistance and an evident separation of the diagram into two semicircles: a high frequency (*hf*) one, with relaxation frequency $f_0 hf \sim 10^6$ Hz, associated with the grain (bulk) resistance, and a low frequency (*lf*) one, which is the characteristic IS response due to the blocking of oxide ions by grain boundaries, pores, or insulating phases in zirconia electrolytes [19]. The IS data clearly reflect the microstructural evolution during sintering of the YSZ ceramic with the blocking of charge carriers being progressively suppressed with increasing temperature. Such a trend is associated with pore elimination and grain growth during sintering of the ceramic specimens. In addition, samples with $m > 0$ display, along with the microstructural evolution during sintering, features associated with the solid solution formation between the two oxides. The IS diagrams of the sample with $m = 30$ (Fig. 1b) present a similar trend: the electrical resistance decreases as the green compact is sintered at high temperatures. However, in this case, semicircles are more convoluted and their separation, seen as a deviation at high frequency, starts at $T \sim 1100$ °C. At higher sintering temperatures, a clearer separation of semicircles occurs and the decrease of the *Rtot* is mostly attributed to the decrease of the low frequency component (*Rlf*), notably at sintering temperatures ≥1150 °C.

X-ray diffraction analysis of YSZ–*m*MgO samples sintered at 1350 °C, revealed that MgO goes into solid solution and that the solubility limit is $m \sim 10$ [13]. It has been previously reported that MgO favors grain growth of YSZ for added concentrations below the solubility limit ($m \leq 10$). Conversely, MgO content exceeding the solubility limit inhibits YSZ grain growth, and samples with $m > 10$ were found to have higher porosity (~80% of the theoretical value) [13]. Nonetheless, the presented IS analysis is assumed to be mostly influenced by both the sintering and the solid solution formation in the YSZ–*m*MgO system.

The evolution of IS diagrams and its relation with microstructural properties of the samples are better visualized in Fig. 2, which shows

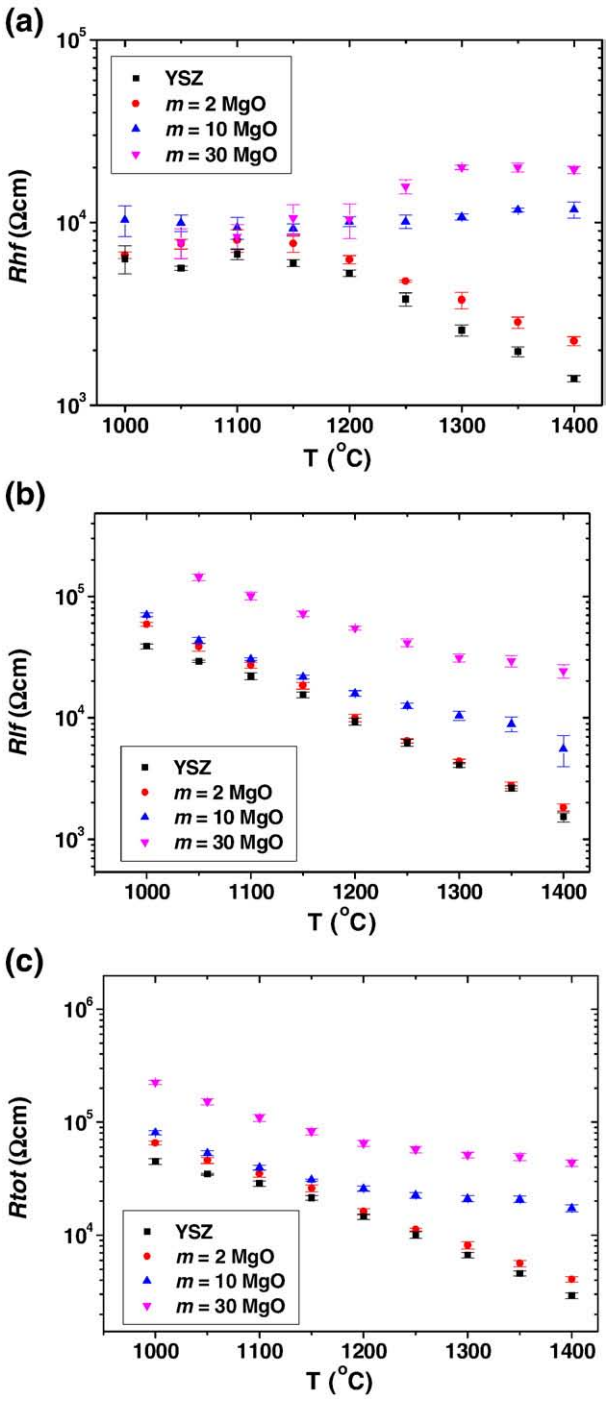

Fig. 2. Electrical resistance components of the samples ZrO_2:8 mol% Y_2O_3–*m* MgO as a function of the sintering temperature: (a) high frequency resistance (*Rhf*), (b) blocking low frequency resistance (*Rlf*), and (c) total electrical resistance ($Rtot = Rhf + Rlf$).

the dependence of the fitted electrical resistance components *Rhf*, *Rlf*, and *Rtot* ($Rhf + Rlf$) on the sintering temperature.

The analyses of both *Rhf* and *Rlf* components of the electrical resistance reveal important features. At $T \leq 1100$ °C, *Rhf* exhibits a weak dependence on the temperature and a tendency to higher *Rhf* values for increasing MgO; however, in this temperature range the convoluted diagrams resulted in some scattering of the fitted *Rhf*. For $T \geq 1100$ °C a clear splitting of *Rhf* depending on the MgO content is observed. For samples $m = 0$ and 2, *Rhf* decreases rapidly with increasing temperature. On the contrary, the temperature dependence of *Rhf* for samples with $m = 10$ and 30 display a slight increase in the

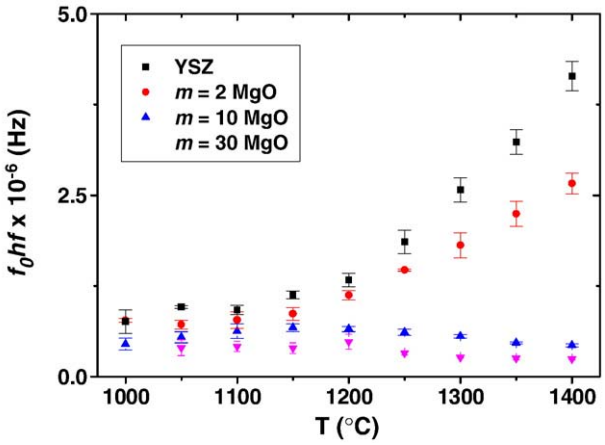

Fig. 3. Temperature dependence of the high frequency relaxation frequency of the ZrO_2:8 mol% Y_2O_3–*m*MgO composites for $m = 0$, 2, 10, and 30.

$T \sim 1150$–1300 °C range. Such a behavior is very important to distinguish different processes occurring in the composite samples: sintering of green compacts and the MgO solubilization into the YSZ matrix. For specimens with $m = 0$ and 2 sintering prevails and *Rhf* clearly reflects the densification of the compacts, as further confirmed by dilatometry analyses (Fig. 4). However, the high frequency resistance (*Rhf*) of samples with MgO addition shows an increase when compared to the one of YSZ that has been associated with the solid solution between MgO and YSZ. The increase of *Rhf* has been related to the reduced mobility of the oxide ions due to defect interactions taking place above the optimal value of the added stabilizer (~8 mol%) [4]. The high frequency resistance also decreases due to a lower volumetric fraction of YSZ with the addition of the insulating phase [19,20].

In contrast to the high frequency component, the blocking resistance *Rlf* continuously decreases with increasing sintering temperature for all specimens, as shown in the Fig. 2b. However, samples with $m \geq 10$ exhibit a slower decrease rate of *Rlf* for $T > 1150$ °C, suggesting that MgO addition modifies the microstructural evolution during sintering, partially remaining as an insulating second phase.

It is interesting to note that initially the compacts are a mixture of YSZ and MgO. When the sintering temperature reaches ~1150 °C, MgO reacts with YSZ, a feature mirrored in the $m = 2$ sample. Below ~1150 °C, the sample with $m = 2$ has *Rhf* values comparable, within the experimental accuracy, to the ones of the $m = 0$ sample. For $T > 1150$ °C, *Rhf* of sample $m = 2$ is clearly increased with respect to the one of the YSZ due to solid solution formation. On the other hand, *Rlf* values for $T < 1150$ °C are higher than that of pure YSZ due to blocking of the oxide ions by the insulating MgO, but for higher temperatures MgO goes into solid solution and both $m = 0$ and 2 samples have similar *Rlf* values. This is a further indication that MgO, added up to the solubility limit ($m < 10$), acts as an insulating blocking phase at low temperatures, and at ~1150 °C it forms a solid solution with YSZ. The data for the samples with $m = 10$ and 30 also reveal relevant information: with increasing sintering temperature the *Rlf* value for the $m = 10$ sample tends to approach the ones of the YSZ, while the *Rhf* value is much higher. In contrast, the *Rlf* of sample $m = 30$ seems to stabilize for sintering temperatures >1300 °C. Such behavior suggests that the solubility limit of MgO in the YSZ matrix is close to 10 mol%, in agreement with previously estimated values [13,21]. The temperature dependence of the total resistance *Rtot* (Fig. 2c) indicates that *Rlf* dominates the electrical behavior during sintering, a feature expected since the contribution of blockers (pores and second phases) are associated with the *lf* component.

The fitted parameters of IS diagrams corresponding to the highest sintering temperature (1400 °C) are within the expected range for both grain and grain boundary values of dense ceramics. At 1400 °C, high frequency capacitance *Chf* values are comparable, in the 2.6 10^{-11}–3.3 10^{-11} F range, and increasing MgO content increases *Chf*. The low frequency *Clf* values for samples with $m \leq 10$ are ~8.0 10^{-10} F, while the sample $m = 30$ has a considerably lower *Clf* ~ 1.0 10^{-10} F, probably due to the presence of MgO and some residual porosity. Decentralization angles were found to be close to the ones measured for zirconia based materials: $\beta hf \sim 6°$, and βlf in the 10–15° range, increasing with increasing MgO content, in agreement with the lower homogeneity of the composite samples [20,22].

The temperature dependence of relaxation frequency (f_0hf), shown in Fig. 3, was analyzed. The relaxation frequency has temperature dependence analogous to the one of *Rhf* (Fig. 2a): all samples display a rather constant value at low temperature and a clear separation between samples with different MgO addition occurs at $T \sim 1150$ °C. A similar dependence of both f_0hf and *Rhf* with sintering temperature was reported for a Bi-based ionic conductor [22]. In that study, f_0hf (*Rhf*) values were found to increase (decrease) in the densification domain, and both parameters reached a constant plateau with increasing sintering temperature that was ascribed as the grain growth regime [22]. In the present work, the absence of a constant plateau of f_0hf at high sintering temperature suggests that the grain growth regime was not attained up to ~1400 °C for samples with low MgO addition ($m = 0$ and 2).

The discussed features of the IS diagrams were further supported by both dilatometry and high temperature X-ray diffraction. The dilatometry analyses of the YSZ–*m*Mg are displayed in Fig. 4 for $m = 0$, 2, and 30. The studied compositions exhibit the onset of the linear shrinkage at $T \sim 1100$ °C, in good agreement with IS data. The linear shrinkage curves for the YSZ and $m = 2$ samples resembles the temperature dependence of the *Rhf* values (Fig. 2a), indicating that the sintering behavior was closely followed by oxide ion conduction, as inferred from the IS data. A maximum shrinkage rate at ~1350 °C was inferred from the peak of the derivative curves and found to be nearly independent on the MgO concentration. However, high MgO content results in decreased total shrinkage at 1500 °C, varying from ~17% for the YSZ to ~14% for the sample with $m = 30$. Apparent densities of samples sintered at 1350 °C showed that up to $m = 10$, the samples have ~90% of the theoretical density. However, increasing MgO addition results in lower density, a feature more pronounced for compositions with $m > 10$. On cooling, the dilatometry curves are essentially linear, and a higher slope is identified in samples with MgO addition.

The high temperature XRD analyses of the $m = 30$ sample revealed that all the observed peaks belong to the cubic phases of yttria-stabilized zirconia and magnesium oxide, as shown in Fig. 5a. No additional phases were detected and the diffraction peaks corresponding to the platinum

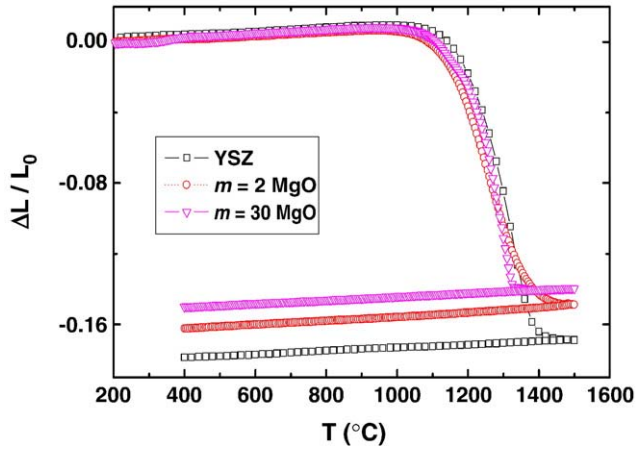

Fig. 4. Linear shrinkage curves of ZrO_2:8 mol% Y_2O_3–*m*MgO composites for $m = 0$, 2, and 30.

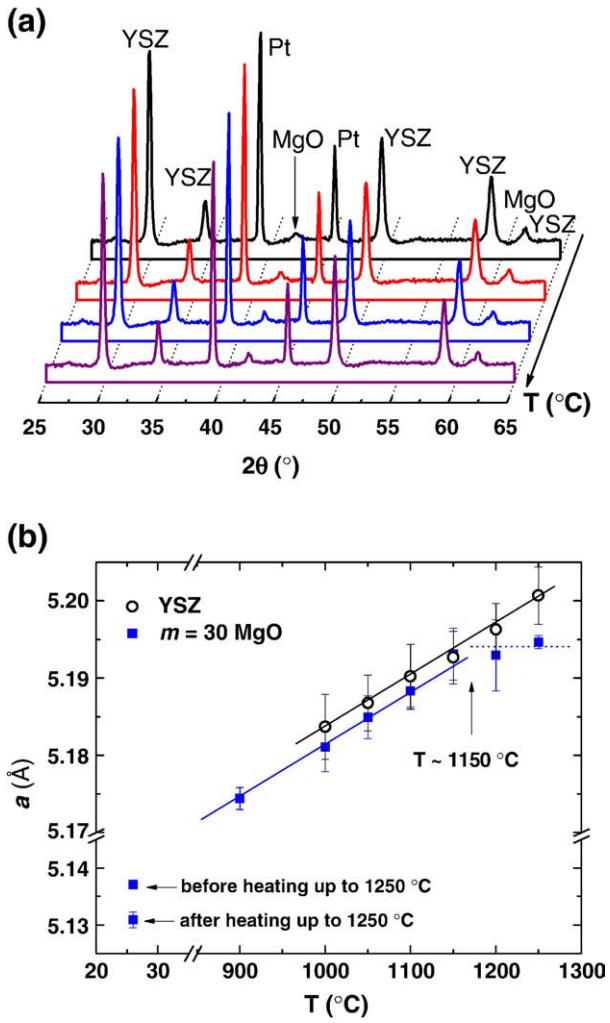

Fig. 5. (a) High temperature X-ray diffraction patterns of ZrO_2:8 mol% Y_2O_3–30 mol% MgO taken at $T = 1000$, 1100, 1200, and 1250 °C. The arrow points towards increasing temperature. (b) Temperature dependence of calculated cubic lattice parameter for samples ZrO_2:8 mol% Y_2O_3–m MgO, with $m = 0$ and 30. Solid lines correspond to linear fittings and the dotted line is a guide for the eye.

sample holder were also measured and used as an internal pattern for XRD data. To further investigate the XRD results, the cubic lattice parameters of YSZ (a) for both the YSZ and the YSZ–30MgO samples were calculated at different temperatures. The temperature dependence of the lattice parameter a is displayed in Fig. 5b for both $m = 0$ and 30 specimens. At room temperature, both samples exhibit $a \sim 5.136$ Å, in good agreement with previously reported values for yttria-stabilized zirconia [23]. Increasing the temperature, both samples have similar values of a, within the experimental error, up to ~1150 °C, and the thermal expansion of the ceramics is observed as a linear dependence of the lattice parameter on the temperature. A rough estimate of the thermal expansion coefficient resulted in values close to $10^{-6}\,K^{-1}$ for both samples, as expected for YSZ, but the $m = 30$ sample presents slightly higher values, in agreement with the dilatometry data (Fig. 4) [12,21]. However, while the lattice parameter of YSZ continues to increase linearly up to 1250 °C, the sample with $m = 30$ deviates from linearity for $T > 1150$ °C. Upon cooling from 1250 °C, the calculated lattice parameter at room temperature $a \sim 5.131$ for the $m = 30$ specimen is smaller than the one determined before heating (Fig. 5b) [13]. Both features of the $m = 30$ sample, i.e., the linear deviation occurring at $T > 1150$ °C and the lower a value after heating, are related to the solid solution formation between YSZ and MgO at high temperature. Moreover, as inferred from the XRD structural parameters, the formation of solid solution between the two oxides was found to occur at essentially the same temperature indicated by the IS data (Fig. 2). At high temperature ($T \geq 1150$ °C), the MgO is soluble in the YSZ matrix, and the lattice parameter decreases with increasing MgO content due to the smaller ionic radius of Mg^{2+} than both the Zr^{4+} and Y^{3+} [24]. Thus, at high temperature, part of the added MgO (up to ~10 mol%) [13,21] forms a solid solution with YSZ and the material is comprised of a co-doped (Y_2O_3 and MgO) zirconia matrix and the remaining MgO as an additional second phase.

4. Conclusion

Impedance spectroscopy was used as a sensitive probe in order to study both sintering and solid solution formation of yttria-stabilized zirconia / magnesia composites. The deconvolution of the frequency-dependent electrical resistance allowed for the determination of several relevant parameters, such as the onset of linear shrinkage and the formation of solid solution between the insulating and the oxide ion conducting phases. Such features were found to be in good agreement with both dilatometry and X-ray diffraction analyses.

Acknowledgments

This work was partially supported by the Brazilian agencies FAPESP and CNPq.

References

[1] E.C. Subbarao, Solid Electrolytes and their Applications, Plenum, New York, 1980, p. 1.
[2] J.H. Lee, J. Mater. Sci. 28 (2003) 4247.
[3] See, for example: S.C. Singhal, K. Kendall, High-temperature Solid Oxide Fuel Cells: Fundamentals, Design and Applications, Elsevier, New York (2004), pp. 1;
L. Blum, W.A. Meulenberg, H. Nabielek, R. Steinberger-Wilckens, Int. J. Appl. Ceram. Technol. 2 (2005) 482;
D.Z. de Florio, J.A. Varela, F.C. Fonseca, E.N.S. Muccillo, R. Muccillo, Quim. Nova 30 (2007) 1339.
[4] J.F. Baumard, P. Abelard, in: N. Claussen, M. Rühle, A.H. Heuer (Eds.), In Science and Technology of Zirconia, vol. II, The American Ceramic Society, Columbus, 1983, p. 555.
[5] R. Muccillo, E.N.S. Muccillo, N.H. Saito, Mater. Lett. 34 (1998) 128.
[6] J. Gong, Y. Li, Z. Tang, Z. Zhang, Mater. Lett. 46 (2000) 115;
V.S. Stubican, J.R. Hellmann, in: A.H. Heuer, L.W. Hobbs (Eds.), Advances in Ceramics, Science and Technology of Zirconia, vol. III, The American Ceramic Society, Columbus, 1981, p. 25;
S.P.S. Badwal, F.T. Ciacchi, S. Rajendran, J. Drennan, Solid State Ionics 109 (1998) 167.
[7] J.R. Hellmann, V.S. Stubican, J. Am. Ceram. Soc. 66 (1983) 260.
[8] R.K. Slotwinski, N. Bonanos, E.P. Butler, J. Mater. Sci. Lett. 4 (1985) 561.
[9] J.-W. Jeong, D.-Y. Yoon, J.-Y. Lee, D.-Y. Kim, J. Am. Ceram. Soc. 75 (1992) 2659.
[10] O.T. Sørensen, M.E.S. Ali, Solid State Ionics 49 (1991) 155.
[11] Z. Jin, V. Du, Ceram. Int. 20 (1994) 17.
[12] Y. Shiratori, F. Tietz, H.P. Buchkremer, D. Stöver, Solid State Ionics 164 (2003) 27.
[13] F.C. Fonseca, R. Muccillo, Solid State Ionics 131 (2000) 301.
[14] M.C. Steil, F. Thevenot, M. Kleitz, J. Electrochem. Soc. 144 (1997) 390.
[15] D.Z. de Florio, R. Muccillo, Solid State Ionics 123 (1999) 301.
[16] F.C. Fonseca, D.Z. de Florio, V. Esposito, E. Traversa, E.N.S. Muccillo, R. Muccillo, J. Electrochem. Soc. 153 (2006) A354.
[17] M. Kleitz, J.H. Kennedy, in: P. Vashishta, J.N. Mundy, G.K. Shenoy (Eds.), Fast Ion Transport in Solids, Electrodes and Electrolytes, North-Holland, Amsterdam, 1979, p. 185.
[18] See, for example, M.M.R. Boutz, A.J.A. Winnubst, A.J. Burggraaf, J. Eur. Ceram. Soc. 13 (1994) 89; S.P.S. Badwal, J. Drennan, J. Mater. Sci. 22 (1987) 3231.
[19] M. Kleitz, L. Dessemond, M.C. Steil, Solid State Ionics 75 (1995) 107.
[20] F.C. Fonseca, R. Muccillo, Solid State Ionics 166 (2004) 157.
[21] Y. Shiratori, F. Tietz, H.J. Penkalla, J.Q. He, Y. Shiratori, D. Stöver, J. Power Sources 148 (2005) 32.
[22] M. Benkaddour, P. Conflant, M. Drache, M.C. Steil, Solid State Ionics 146 (2002) 175.
[23] ICDD file no. 30-1468.
[24] R.D. Shanon, Acta Crystallogr. A32 (1976) 751.